1

Molecule-Based Magnetic Coolers: Measurement, Design and Application

Marco Evangelisti

Instituto de Ciencia de Materiales de Aragón, CSIC – Universidad de Zaragoza, Departamento de Física de la Materia Condensada, 50009 Zaragoza, Spain
m.e@csic.es

Abstract. The recent progress in molecule-based magnetic materials exhibiting a large magnetocaloric effect at liquid-helium temperatures is reviewed. The experimental methods for the characterization of this phenomenon are described. Theory and examples are presented with the aim of identifying those parameters to be addressed for improving the design of new refrigerants belonging to this class of materials. Advanced applications and future perspectives are also discussed.

1.1 Introduction

Magnetic refrigeration exploits the magnetocaloric effect (MCE), which can be described as either an isothermal magnetic entropy change (ΔS_m) or an adiabatic temperature change (ΔT_{ad}) following a change of the applied magnetic field (ΔH). The roots of this technology date back to 1881, when Warburg experimentally observed that an iron sample heated a few milliKelvin when moved into a magnetic field and cooled down when removed out of it [1]. In 1918, Weiss and Piccard explained the magnetocaloric effect [2]. In the late 1920s, Debye and Giauque independently proposed adiabatic demagnetization as a suitable method for attaining sub-Kelvin temperatures [3, 4]. In 1933, Giauque and MacDougall applied this method to reach 0.25 K by making use of 61 grams of $Gd_2(SO_4)_3 \cdot 8H_2O$, starting from 1.5 K and applying $\mu_0 \Delta H = 0.8$ T [5]. Since then, magnetic refrigeration is a standard technique in cryogenics, which has shown to be useful to cool down from a few Kelvin [6, 7]. Applications include, among others: superconducting magnets, helium liquifiers, medical instrumentation, in addition to many scientific researches. So-called adiabatic demagnetization refrigerators (ADR) are used as ultra-low-temperature platforms in space borne missions, where the absence of gravity prevents cooling by methods based on ^{3}He-^{4}He dilutions. Magnetic refrigeration at liquid-helium temperatures provides a valid alternative to the

use of helium itself, specially for the rarer ^{3}He isotope, whose cost has been increasing dramatically during the past few years.

All magnetic materials show the MCE, although the intensity of the effect depends on the properties of each material. Since the initial proposition that magnetic molecular clusters are promising systems for refrigeration at low temperatures [8], very large values of ΔS_m and ΔT_{ad} have been repeatedly reported for several molecule-based magnetic materials. Table 1.1 lists a wide up-to-date selection of such refrigerants, with their corresponding references. An extensive investigation is currently under way, with a view to finding or synthesizing new molecule-based materials capable of record performances in terms of the MCE.

In order to efficiently exploit the MCE for a realistic application, this effect should be maximized within the working temperature range of interest. In order to do so at cryogenic temperatures, the molecule-based magnetic coolers must possess a combination of a large spin ground state with negligible anisotropy, weak ferromagnetic exchange between the constituent magnetic ions, in addition to a relatively large metal:non-metal mass ratio, i.e., a large magnetic density. This chapter describes the underlying physics of magnetic refrigeration with molecule-based coolers. Section 1.2 defines the MCE and provides its theoretical framework. Section 1.3 addresses which experimental techniques should be applied, and how to correctly do it, in order to characterize the MCE of this class of materials. Several case examples are provided in section 1.4, with the aim of highlighting the characteristics which are known to influence the performance of these coolers. Section 1.5 introduces the reader into the field of on-chip microrefrigeration – an advanced application which starts from the challenging magnetic characterization of molecule-based magnetic coolers deposited over a substrate. Concluding remarks are presented in section 1.6.

1.2 Theoretical Framework

In order to explain the origin of the magnetocaloric effect, we use thermodynamic relations which relate the magnetic variables (magnetization M and magnetic field H) to entropy S_E and temperature T. Let us recall [55] that the definition of the entropy of a system having Ω accessible states is $S_E = k_B \ln(\Omega)$. Since a magnetic moment of spin s has $2s + 1$ magnetic spin states, the entropy content per mole of substance associated with the magnetic degrees of freedom at $T = \infty$ is

$$S_m = R \ln(2s + 1), \tag{1.1}$$

where $R = N_A k_B$ is the gas constant. The spin s should be considered as an effective spin describing the multiplicity of relevant magnetic states.

When a material is magnetized by the application of a magnetic field, the magnetic entropy is changed as the field changes the magnetic order of the

Table 1.1. Selection of molecule-based magnetic refrigerants and corresponding references. A rough chronological order is followed from top to bottom

Compound	Ref.	Compound	Ref.
$\{Mn_{12}\}$	[9]	$\{Fe_8\}$	[9]
$\{Cr_7Cd\}$	[10]	$\{Fe_{14}\}$	[11–13]
$\{NiCr\}_n$	[14, 15]	$\{Cr_3Gd_2\}_n$	[14, 15]
$\{Mn_6^{3+}Mn_4^{2+}\}$	[16]	$\{Mn_6^{3+}Mn_4^{2+}\}$	[17]
$\{Mn_6^{3+}Mn_8^{2+}\}$	[17]	$\{Mn_4^{3+}Gd_4\}$	[18, 19]
$\{Mn_8^{4+}Mn_{24}^{2+}\}$	[20]	$[Gd_2(fum)_3(H_2O)_4]\cdot 3H_2O$	[21]
$\{Mn_6^{3+}Mn_4^{2+}\}$	[22]	$\{Mn_{11}^{3+}Mn_6^{2+}\}$	[22]
$\{Mn_{12}^{3+}Mn_7^{2+}\}$	[22]	$\{Gd_7\}$	[23]
$\{Mn_{19}\}$	[24]	$\{Na_2Mn_{15}\}$	[24]
$\{Ni_6Gd_6P_6\}$	[25]	$\{Ni_{12}Gd_{36}\}$	[26]
$\{Co_6Gd_8\}$	[26]	$[Gd_2(OAC)_6(H_2O)_4]\cdot 4H_2O$	[27, 28]
$\{Cu_5Gd_4\}$	[29]	$\{Ni_3Gd\}$	[30]
$\{Co_8Gd_8\}$	[31]	$\{Co_4Gd_6\}$	[31]
$[Gd_2(OAC)_3(H_2O)_{0.5}]_n$	[32]	$[Gd_4(OAC)_4(acac)_8(H_2O)_4]$	[32]
$[Gd_2(OAC)_3(MeOH)]_n$	[32]	$[Gd_2(OAC)_2(Ph_2acac)_6(MeOH)_2]$	[32]
$\{Co_4Gd_6\}$	[33]	$\{Co_8Gd_4\}$	[33]
$\{Co_4Gd_2\}$	[33]	$\{Co_8Gd_2\}$	[33]
$\{Co_8Gd_8\}$	[33]	$\{Co_8Gd_4\}$	[33]
$\{Fe_5Gd_8\}$	[34]	$\{Cu_{36}Gd_{24}\}$	[35]
$\{Gd_{10}\}$-POM	[36]	$\{Gd_{30}\}$-POM	[36]
$\{Zn_8Gd_4\}$	[37]	$\{Ni_8Gd_4\}$	[37]
$\{Cu_8Gd_4\}$	[37]	$\{Gd_5Zn(BPDC)_3\}_n$	[38]
$\{Cr_2Gd_3\}$	[39]	$\{Cr_2Gd_2\}$	[40]
$\{Co_{10}Gd_{42}\}$	[41]	$\{Ni_{10}Gd_{42}\}$	[41]
$[Gd_2(N\text{-}BDC)_3(dmf)_4]$	[42]	$[Mn(H_2O)_6][MnGd(oda)_3]_2\cdot 6H_2O$	[43]
$\{Cu_6^{2+}Gd_6^{3+}\}$	[44]	$Co_4(OH)_2(C_{10}H_{16}O_4)_3$	[45]
$\{NiNb^{4+}\}_n$	[46]	$\{Mn^{2+}Nb^{4+}\}_n$	[46]
$[Gd(HCOO)(C_8H_4O_4)]$	[47]	$\{Gd_{12}Mo_4\}$	[48]
$\{Fe_{17}\}$	[49]	$\{Gd_{24}\}$	[50]
$\{Ni_{12}Gd_5\}$	[51]	$\{Co_6Gd_4\}$	[52]
$\{Gd(OOCH)_3\}_n$	[53]	$\{MnGd\}$	[54]

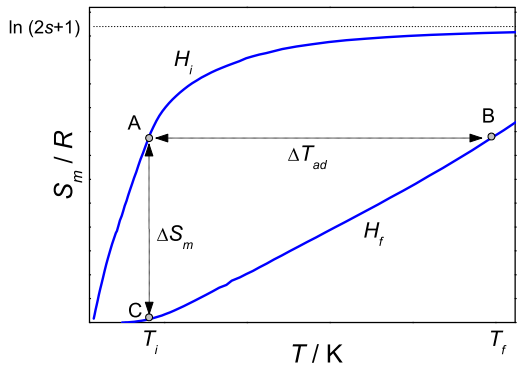

Fig. 1.1. Temperature-dependence of the molar magnetic entropy of a (super)paramagnet with spin s per formula unit, for magnetic field H_i and $H_f > H_i$. AB process: adiabatic magnetization (A $\rightarrow$ B) or demagnetization (B $\rightarrow$ A), providing ΔT_{ad}. AC process: isothermal magnetization (A $\rightarrow$ C) or demagnetization (C $\rightarrow$ A), providing ΔS_m

material. The MCE and the associated principle of adiabatic demagnetization is readily understood by looking at Figure 1.1. The system, assumed to be a paramagnetic material, is initially in state A(T_i, H_i), at temperature T_i and field H_i. Under adiabatic conditions, i.e., when the total entropy of the system remains constant, the magnetic entropy change must be compensated for by an equal but opposite change of the entropy associated with the lattice, resulting in a change in temperature of the material. That is, the adiabatic field change $H_i \rightarrow H_f$ brings the system to state B(T_f, H_f) with the temperature change $\Delta T_{ad} = T_f - T_i$ (horizontal arrow in Fig. 1.1). On the other hand, if the magnetic field is isothermally changed to H_f, the system goes to state C(T_i, H_f), resulting in the magnetic entropy change ΔS_m (vertical arrow). Both ΔS_m and ΔT_{ad} are the characteristic parameters of the MCE. It is easy to see that if the magnetic change ΔH reduces the entropy ($\Delta S_m < 0$), then ΔT_{ad} is positive, whereas if ΔH is such that $\Delta S_m > 0$, then $\Delta T_{ad} < 0$.

1.3 Experimental Evaluation of the MCE

A widely-accepted approach used to evaluate the MCE consists in obtaining ΔS_m exclusively from magnetization measurements as function of temperature and applied magnetic field, by adopting the procedure described in Sect. 1.3.1. Although some care should be taken for collecting and then analyzing the experimental data correctly, this approach has the clear advantages of being simple and relatively fast. No other experimental tool is needed but a

conventional magnetometer. A far more complete characterization of the MCE is accomplished by means of heat capacity measurements collected for varying temperature and applied magnetic field, which permit to compute both ΔS_m and ΔT_{ad}. For the practical cases, these two *indirect* approaches rely on the numerical evaluation of integrals that, by their nature, can produce heavy errors, as made evident by Pecharsky and Gschneidner [56]. To overcome any inherent shortfall, a third and more reliable option is the *direct* measurement of the physical effect. Although several experimental methods succeeded in measuring directly the MCE, a higher degree of sophistication is required and therefore this option is restricted within a few specialized laboratories.

1.3.1 Indirect Methods

In order to establish the relationship between H, M and T to the MCE terms, ΔT_{ad} and ΔS_m, we consider the Maxwell equation for the magnetic entropy

$$\left(\frac{\partial S_m(T,H)}{\partial H}\right)_T = \left(\frac{\partial M(T,H)}{\partial T}\right)_H. \tag{1.2}$$

Integrating Eq. 1.2 for an isothermal process, we obtain

$$\Delta S_m(T,\Delta H) = \int_{H_i}^{H_f} \left(\frac{\partial M(T,H)}{\partial T}\right)_H \mathrm{d}H. \tag{1.3}$$

This equation indicates that ΔS_m is proportional to both the derivative of magnetization with respect to temperature at constant field and to the field variation. The accuracy of ΔS_m calculated from magnetization experiments using Eq. 1.3 depends on the accuracy of the measurements of the magnetic moment, T and H. It is also affected by the fact that the exact differentials are replaced by the measured variations (ΔM, ΔT and ΔH). Furthermore, it is worth mentioning that the Maxwell equation does not hold for first order phase transitions, since $\partial M/\partial T \to \infty$.

By replacing the specific heat at constant field

$$C = T\left(\frac{\partial S_m}{\partial T}\right)_H,$$

in the expression of the infinitesimal change of $S_m(T,H)$, we have

$$\mathrm{d}S_m = \left(\frac{\partial S_m}{\partial T}\right)_H \mathrm{d}T + \left(\frac{\partial S_m}{\partial H}\right)_T \mathrm{d}H = \frac{C}{T}\mathrm{d}T + \left(\frac{\partial S_m}{\partial H}\right)_T \mathrm{d}H. \tag{1.4}$$

For an adiabatic process, $\mathrm{d}S_m = 0$. Thus, we obtain

$$\mathrm{d}T_{ad} = -\frac{T}{C}\left(\frac{\partial S_m}{\partial H}\right)_T \mathrm{d}H, \tag{1.5}$$

where T_{ad} is the adiabatic temperature. Therefore, taking into account Eq. 1.2, the adiabatic temperature change is expressed by

$$\Delta T_{ad}(T, \Delta H) = \int_{H_i}^{H_f} \left(\frac{T}{C(T,H)}\right)_H \left(\frac{\partial M(T,H)}{\partial T}\right)_H \mathrm{d}H. \tag{1.6}$$

From the experimental specific heat, the temperature dependence of the magnetic entropy $S_m(T)$ is obtained by integration, i.e., using

$$S_m(T) = \int_0^T \frac{C_m(T)}{T} \mathrm{d}T, \tag{1.7}$$

where $C_m(T)$ is the magnetic specific heat as obtained by subtracting the lattice contribution from the total measured C. Hence, if $S_m(T)$ is known for H_i and H_f, both $\Delta T_{ad}(T, \Delta H)$ and $\Delta S_m(T, \Delta H)$ can be obtained.

The accuracy in the evaluation of MCE using specific heat data depends critically on the accuracy of the C measurements and data processing, e.g., the use of ΔT instead of $\mathrm{d}T$. Indeed, small errors in C can produce important differences in ΔS_m and ΔT_{ad} at high temperature due to the integration process. Moreover, C data measured by the heat pulse technique are less accurate near phase transitions due to the long relaxation times required for thermal equilibrium after each pulse. An additional source of uncertainty may eventually come from the fact that, in order to carry out the integration of Eq. 1.7, one has to extrapolate the experimental data to $T = 0$ and to $T = \infty$. The former extrapolation might become critical depending on the lowest experimentally-accessible temperature in comparison to the magnitude of the relevant energies involved in the magnetic ordering mechanism due to, e.g., interactions that are typically weak in molecule-based magnetic materials. For a magnetic system that undergoes a phase transition within the accessible T window, one can sometimes attempt the extrapolation to $T = 0$ by making use of spin-wave models [20]. Alternatively, the 'missing' entropy that characterizes the not-accessible lowest temperatures can be estimated from the expected full entropy content (Eq. 1.1), after subtracting the result obtained by integrating Eq. 1.7 between the experimental lowest T and the high-T extrapolation ($\propto T^{-2}$). However, one has to consider that the drawback of such a method is an increasingly large uncertainty, which might jeopardize and even invalidate the analysis based on the specific heat data. For a molecule-based refrigerant containing Gd^{3+} spin centers, the zero-field magnetic specific heat shows up for temperatures lower than $2 - 3$ K. It is then not sufficient to use a commercial calorimeter typically limited to ≈ 2 K as the lowest achievable T by pumping ^{4}He. An unfortunate example of poor analysis of specific heat data can be spotted in the recent literature [41]. As a rule of thumb, if the molecule-based refrigerant contains Gd^{3+} spin centers, then sub-Kelvin temperatures are needed for characterizing the MCE by specific heat experiments.

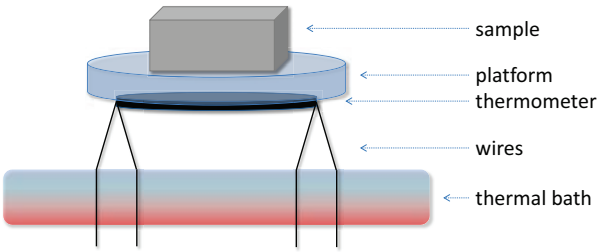

Fig. 1.2. Scheme of the thermal sensor used for the direct determination of the temperature change on magnetization and demagnetization

1.3.2 Direct Measurements

A far more elegant and reliable method for determining the MCE is by means of *direct* measurements. Clearly, the advantage resides in avoiding those drawbacks inherent to indirect methods, such as the poor accuracy associated to the data processing and the $T \rightarrow 0$ extrapolation of the specific heat (see section 1.3.1). However, any experimental set-up designed for direct MCE measurements has to deal with unavoidable heat dissipations, i.e., the lack of ideal adiabatic conditions. Most employed methods are based on a rapid change of the applied magnetic field during the, correspondingly short, time interval of a single measurement [57]. These measurements could be considered adiabatic experiments, at least to a first approximation. In the procedure described below, we go beyond this time interval by providing a full description of the physical process involved, which becomes relevant at a scale longer than the time needed for fully changing the applied field [27, 53].

In the experimental set-up, the sample-holder is a sapphire plate to which a resistance thermometer is attached (Figure 1.2). The wires provide electrical connection, mechanical support and thermal contact to a controlled thermal bath at constant temperature T_0. Starting with the sample at zero field $H = 0$ and T_0, the measuring procedure comprises the following four steps: a) gradual application of a magnetic field, up to a maximum H_0; b) relaxation until the sample reaches again the thermal equilibrium with the bath; c) gradual demagnetization down to $H = 0$; d) relaxation at zero field until the sample reaches the equilibrium at T_0. During the whole procedure, the as-measured temperature T and applied magnetic field H are recorded continuously.

In order to cope with the unavoidable lack of ideal adiabaticity, one has to relate the as-measured T to the adiabatic temperature T_{ad}, i.e., the temperature if the sample would have been kept thermally isolated during the process. For this purpose, the experimental entropy gains (losses) of the sample which originate from heat dissipation from (to) the thermal bath should be evaluated. The thermal conductance κ of the wires is previously measured as a function of the temperature using a free-oxygen copper block as the sam-

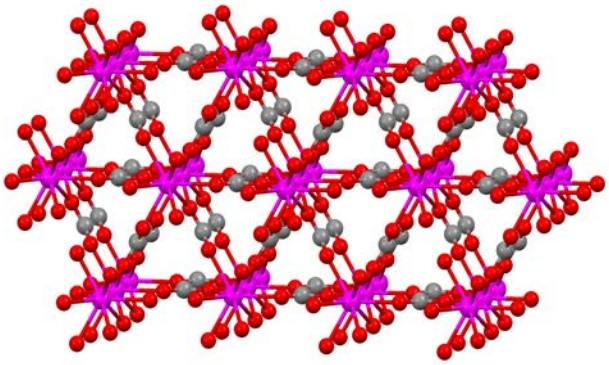

Fig. 1.3. Structure of the $\{Gd(OOCH)_3\}_n$ three-dimensional metal-organic framework material. Gd = purple, O = red, C = gray. H atoms are omitted for clarity

ple. The specific heat at constant field, C, of the sample is also previously measured using another calorimeter.

The entropy change of the sample in an infinitesimal time interval is

$$\mathrm{d}S = \frac{k(T_0 - T)}{T}\mathrm{d}t. \tag{1.8}$$

Taking into account Eq. 1.4, we then have

$$\begin{aligned} \frac{k(T_0 - T)}{T}\mathrm{d}t &= \frac{C}{T}\mathrm{d}T + \left(\frac{\partial S}{\partial H}\right)_T \mathrm{d}H, \\ \frac{\mathrm{d}T}{\mathrm{d}t} &= \frac{k(T_0 - T)}{C} - \frac{T}{C}\left(\frac{\partial S}{\partial H}\right)_T \frac{\mathrm{d}H}{\mathrm{d}t}. \end{aligned} \tag{1.9}$$

By replacing $\mathrm{d}T_{ad}$ from Eq. 1.5, we obtain

$$\frac{\mathrm{d}T}{\mathrm{d}t} = \frac{k(T_0 - T)}{C} + \frac{\mathrm{d}T_{ad}}{\mathrm{d}t},$$

which finally results in

$$T_{ad}(t) = T(t) - \int_{t_0}^{t} \frac{k(T_0 - T)}{C}\mathrm{d}t. \tag{1.10}$$

Therefore, knowing κ and C, the adiabatic temperature can be precisely determined for the whole magnetization-demagnetization process. From Eq. 1.10, we note that the deviation of $T(t)$ from $T_{ad}(t)$, as in the ideal adiabatic process, increases with t. We then also note that $T(t) \simeq T_{ad}(t)$ when $t/t_0 \simeq 1$. Thus, if the measurement is based on a fast change of the applied magnetic field and it is limited to the short time scale corresponding to

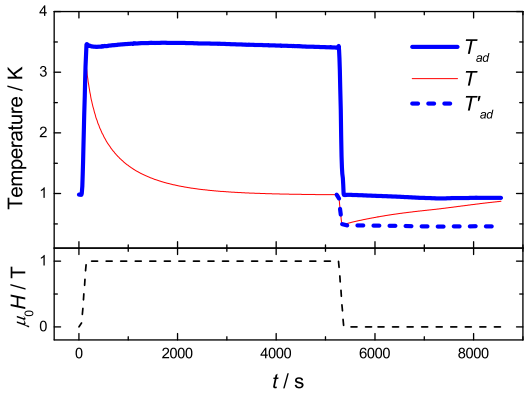

Fig. 1.4. Top: Direct measurement of the experimental temperature T and deduced adiabatic temperatures T_{ad} and T'_{ad} for $\{Gd(OOCH)_3\}_n$ on a magnetization and demagnetization cycle. Bottom: Time evolution of the corresponding applied magnetic field

the interval needed for fully changing the applied field, then the as-measured T already provides a good determination of the adiabatic temperature. In this treatment, the entropy contribution due to the heat transferred from the sample holder to the refrigerant material, i.e., $\Delta S_{sh} = \int_{T_0}^{T} C_{sh}/T \mathrm{d}T$, is disregarded. This is acceptable since the specific heat of the sample holder C_{sh} typically is orders of magnitude lower, and therefore negligible, with respect to that of the sample at these liquid-helium temperatures.

Case Example: $\{Gd(OOCH)_3\}_n$ *3D Metal-Organic Framework*

Hereafter, we describe the direct measurements of the temperature changes, induced by ΔH, that were reported in Ref. [53] for gadolinium formate, whose chemical formula is $\{Gd(OOCH)_3\}_n$, which belongs to the class of metal-organic framework (MOF) materials (Figure 1.3).

For $\{Gd(OOCH)_3\}_n$, Figure 1.4 shows the time evolution of the field H, experimental temperature T and deduced adiabatic temperature T_{ad} for a representative magnetization-demagnetization full cycle, starting at $T_0 = 0.98$ K and reaching $\mu_0 H_0 = 1$ T. In sequential order, we can observe the following stages. The experimental temperature T increases while the field increases up to 1 T. Here T_{ad} increases more than T because the thermal losses to the bath are compensated to compute T_{ad}. The experimental temperature T decays back to $T_0 = 0.98$ K, but $T_{ad} = 3.5$ K is constant, since it corresponds to an hypothetical adiabatic process at constant H. In the demagnetization process, starting from $t_0 = 5270$ s in Fig. 1.4, T decreases below T_0 due to the magnetocaloric effect (section 1.2). By 'resetting' T_0 to 0.98 K, we can here define a new, though equivalent, adiabatic temperature T'_{ad} (dashed line in

the top panel). We observe that T_{ad} tends to recover the initial value T_0 corresponding to $t_0 = 0$, while T'_{ad} cools down to the new temperature of 0.47 K because of the MCE. Then, the experimental temperature T gradually relaxes back to the equilibrium value, while T_{ad} and T'_{ad} are constant. Specifically, T_{ad} is equal to the starting $T_0 = 0.98$ K for $t_0 = 0$, since the real entropy gain is exactly compensated for by the calculation. The fact that the final temperature T tends to agree with T_{ad} after demagnetization, indicates that entropy gains and losses have been correctly estimated throughout the whole process. Remarkably, the final adiabatic temperatures of 3.5 K and 0.47 K obtained after sweeping the 1 T field up and down, respectively, corroborate the results independently inferred from indirect methods [53].

Recollecting the discussion on the adiabaticity and its lack thereof, we finally note that the use of Eq. 1.10 is not essential if the MCE is sufficiently large, as for $\{Gd(OOCH)_3\}_n$, and the measuring time does not exceed the time needed for fully changing H. For instance for the above-mentioned demagnetization process, the as-measured T is 0.48 K at the precise time in which the field reaches zero value (i.e., $t = 5370$ s in Fig. 1.4). From Eq. 1.10, we obtain the corresponding $T_{ad} = 0.47$ K - thus equivalent to a 2% correction, only. This means that the measured cooling for $T = 0.48$ K and $\mu_0 \Delta H_0 = (1 - 0)$ T is given by $\Delta T = (0.98 - 0.48)$ K $= 0.50$ K, which is corrected to $\Delta T_{ad} = 0.51$ K after applying Eq. 1.10. Therefore, we conclude that this type of experiments can provide a direct estimate of the parameters which characterize the MCE.

1.4 Designing the Ideal Refrigerant

This section addresses the parameters which are known to influence the performance of a molecule-based material as a cryogenic refrigerant. We anticipate that the design of the ideal refrigerant requires the optimization of the following items:

- magnetic anisotropy,
- type and strength of the magnetic interactions,
- relative amount of non-magnetic ligand elements.

One further criterium to be considered is the type of spins involved since the magnetic entropy is determined by the spin according to Eq. 1.1. In this respect, gadolinium is the preferred constituent element because its $^8S_{7/2}$ ground state provides the largest entropy per single ion. Furthermore, it has no orbital angular momentum contribution to the ground state. This implies that its full magnetic entropy R ln (8), corresponding to a spin value $s = 7/2$, is readily available at liquid-helium temperatures. For the same reason, Mn^{2+} and Fe^{2+} ions are also often used for the synthesis of molecule-based refrigerants because of their next largest 5/2 spin value.

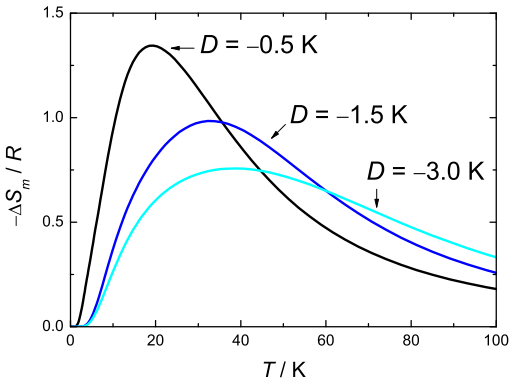

Fig. 1.5. Magnetic entropy changes ΔS_m, normalized to the gas constant R, calculated for spin $s = 10$ and varying anisotropy $D = -0.5$ K, -1.5 K and -3.0 K, following an applied field change of $\mu_0 \Delta H = (7 - 1)$ T

1.4.1 Magnetic Anisotropy

In addition to a large spin value, another condition that favors a large MCE is a relatively small magnetic anisotropy. The crystal-field effects arising from the metal oxidation states and surrounding organic ligands, concurrently with anisotropic magnetic interactions, set in a preferential direction for the spins. The larger is this anisotropy, the less sensitive to H is the polarization of the spins, or (equivalently) higher fields are needed, therefore yielding a lower MCE. This concept is further explained by the following example which is based on observing the evolution of the Schottky specific heat $C_{\rm Sch}$ as a function of temperature, field and anisotropy. Let us mention that the Schottky anomaly for a finite set of energy levels E_i and corresponding degeneracies g_i is defined by the expression

$$C_{\rm Sch} = \left(\frac{1}{k_B T}\right)^2 \frac{\sum_{i,j} g_i g_j (E_i^2 - E_i E_j) \exp[-(E_i + E_j)/k_B T]}{\sum_{i,j} g_i g_j \exp[-(E_i + E_j)/k_B T]}. \qquad (1.11)$$

We consider a *hypothetical* fixed value $s = 10$ for the spin, while we vary the axial anisotropy as such to be $D = -0.5$ K, -1.5 K and -3.0 K. First, for each D we calculate the Schottky heat capacities $C_{\rm Sch}$ from Eq. 1.11 for two different values of the applied field, e.g., $\mu_0 H_i = 1$ T and $\mu_0 H_f = 7$ T. Then, we obtain the corresponding magnetic entropies $S_m(T, H)$ by making use of Eq. 1.7. As depicted in Fig. 1.1, we finally deduce the magnetic entropy changes $\Delta S_m(T, \Delta H) = [S_m(T, H_f) - S_m(T, H_i)]$ for the applied field change $\mu_0 \Delta H = (7 - 1)$ T. Figure 1.5 shows that the resulting T-dependence of $-\Delta S_m$ shifts to higher temperatures and, overall, decreases to lower values by increasing the value of D. Therefore, we can conclude that, if we target the

highest MCE, we should design the molecule-based material as such to present the lowest anisotropy, which would permit the easy polarization of the spins in order to yield a large magnetic entropy change. This also demonstrates that, in order to be successful, the applicability of the (isotropic) molecule-based materials has to be at very low temperatures.

1.4.2 Magnetic Interactions

A common strategy to optimize the MCE is by playing with the magnetic interactions since these set the way in which the magnetic entropy is released as a function of temperature. Let us present the physics involved in the way in which magnetic ordering can lead to a partial concentration of the total magnetic entropy change into a limited range of temperature. For the sake of simplicity, we assume a magnetically-isolated molecule with a total spin $S_{\rm tot} = ns$ for a finite number n of spins s, which are part of the same molecule. If it is paramagnetic, with n non-interacting spins s, the magnetic entropy per mole is

$$S_m = n\ R\ \ln(2s+1), \tag{1.12}$$

from Eq. 1.1. However, at low temperatures where the n spins s couple into $S_{\rm tot} = ns$, the entropy to consider is $S'_m = R\ \ln(2S_{\rm tot}+1) = R\ \ln(2ns+1)$, which is clearly different. Obviously the total magnetic entropy gain that can be reached between zero and *infinite* temperature remains equal to S_m, which is the maximum entropy gain. What does change is the way in which the magnetic entropy is released as a function of temperature. Indeed, the temperature dependence of the magnetic entropy shows a smooth gradual increase from zero at $T = 0$ to the maximum $R\ \ln(2s+1)$ in the paramagnetic case, while it changes into a more steep dependence in the temperature range where the interactions become important. This can be used advantageously to produce a large ΔS_m by means of a limited change in T and/or H, that is, a much larger change than can be produced in the absence of such interactions.

We note that the aforementioned argument is conceptually analogous for a bulk solid-state material. In the case of a magnetic phase transition at a critical temperature T_C, one could in principle play the same game, i.e., enhancing the entropy change in proximity of T_C by small changes in field or temperature. For most high-temperature solid-state refrigerant materials, the MCE is indeed driven by the mechanism of magnetic ordering [57], and so is also for molecule-based materials, namely Prussian blue analogues [14, 15]. In the case of liquid-helium temperatures, thermal fluctuations are typically stronger than magnetic fluctuations arising from intermolecular interactions, especially when the material contains Gd^{3+} spin centres. Therefore for such systems, one would expect the magnetic dimensionality to play no dominant role in the MCE, unless experiments are carried out deep in the sub-Kelvin regime [36]. We finally note that a drawback inherent to any magnetic phase transition is that the MCE steeply falls to near zero values below T_C, limiting

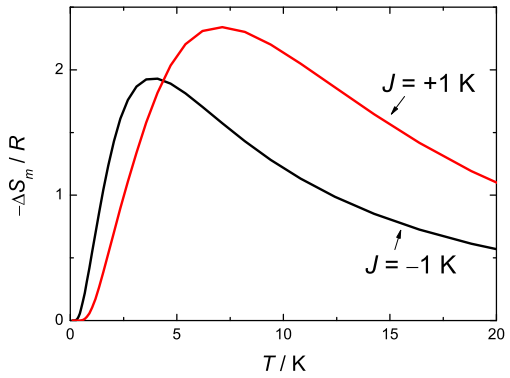

Fig. 1.6. For a dimer of spins $s_{1z} = s_{2z} = 7/2$, calculated magnetic entropy changes ΔS_m, normalized to the gas constant R, obtained for exchange constant $J = +1$ K (ferromagnetic interaction) and $J = -1$ K (antiferromagnetic interaction) following an applied field change $\mu_0 \Delta H = (7 - 1)$ T

the lowest temperature which can be attained in a process of adiabatic demagnetization. Therefore, particular attention should be devoted to 'control' the magnetic interactions depending on the target working temperature of the magnetic refrigerant.

Sign of Exchange Interaction

The MCE is heavily influenced by the type of magnetic interactions involved. This is particularly true in the case of antiferromagnetic interactions that tend to contribute negatively to the physical effect. To shed some light, let us present the model of a dimer of spins $\mathbf{s_1}$ and $\mathbf{s_2}$ that are magnetically coupled to each other by an exchange constant J. As a simplification, we restrict the spins to point along a z direction and we assume $s_{1z} = s_{2z} = 7/2$. Therefore, the Ising Hamiltonian accounting for the magnetic exchange and a Zeeman interaction is given by

$$\mathcal{H} = -J s_{1z} s_{2z} - g\mu_B (s_{1z} + s_{2z}) H, \tag{1.13}$$

where g is the Landé g-factor and μ_B is the Bohr magneton. Through numerical matrix diagonalization, one can compute the energy levels and eigenvectors, and hence the specific heat, for varying J and H. We consider ferromagnetic and antiferromagnetic exchange either by setting $J = +1$ K or $J = -1$ K, respectively. For each case, the calculation is repeated twice for applied field values $\mu_0 H = 1$ T and $\mu_0 H = 7$ T, respectively. Then by making use of Eq. 1.7, we obtain the magnetic entropy, which straightforwardly leads to the entropy change ΔS_m, depicted in Figure 1.6 for $\mu_0 \Delta H = (7 - 1)$ T and

both ferro- and antiferromagnetic interaction. It is easy to discern that the sign of J is highly relevant in the determination of the MCE, this being larger and shifted to higher temperatures for the case of ferromagnetic coupling. By further increasing ΔH, both ferro- and antiferromagnetic $-\Delta S_m(T, \Delta H)$ curves will gradually increase to ultimately reach the limit of the full entropy content, which corresponds to the entropy of two magnetically-independent spins, i.e. $2 \times R \ln(8) \simeq 4.16\ R$. We note that a larger ΔH is needed in the case of the antiferromagnetic interaction for reaching such a limit. Extrapolating the result of this simulation, we can conclude that ferromagnetism is to be preferred to antiferromagnetism since the former promotes a higher magnetocaloric effect.

Screening by Diluting: Ultra-Low Temperatures

Attaining temperatures in the range of milliKelvin dates back to the very beginning of the research field on cooling by adiabatic demagnetization. For the aforementioned reasons, this goal can only be achieved by avoiding any source of magnetic interactions. Diluted paramagnetic salts, like cerium magnesium nitrate (CMN) and chromic potassium alum (CPA), can achieve mK temperatures favored by the weak strength of the interactions between the paramagnetic ions [6]. However, these commercially-employed magnetic refrigerants are also characterized by a relatively strong magnetic anisotropy and low refrigeration power, which results from the small effective-spin values and spin-to-volume ratios. From Sect. 1.4.1 we have learnt that the lower the anisotropy, the less pronounced are the crystal field effects which, splitting the energy levels, result in MCE maxima at lower temperatures. This leads once again to consider gadolinium as a potentially interesting element for mK cooling. Gadolinium sulfate [5, 58] and gadolinium gallium garnet (GGG) [59, 60] are well-known low-temperature magnetic refrigerants, although they are limited by their magnetic ordering temperatures, and so is the gadolinium acetate tetrahydrate with $T_C \simeq 0.2$ K [27]. Likewise, one may expect a relatively large ordering temperature in the case of extended Gd^{3+}-based systems, such as one-dimensional chains [32]. Mixed Gd^{3+}-Mn^{3+}, Gd^{3+}-Co^{2+}, and Gd^{3+}-Ni^{2+} molecular nanomagnets have been considered as magnetic coolers (see Table 1.1) but they are not suitable for ultra-low temperatures due to the anisotropy induced by the Mn^{3+}, Co^{2+}, and Ni^{2+} ions, respectively.

Case Example: Mononuclear GdW_{10} *and* GdW_{30} *POM Salts*

A recent research has focused on the magnetocaloric properties of two novel molecular nanomagnets based on polyoxometalate (POM) salts with general formula $Na_9[Gd(W_5O_{18})_2] \cdot 35H_2O$ (hereafter shortened as GdW_{10}) and $K_{12}(GdP_5W_{30}O_{110}) \cdot 54H_2O$ (hereafter shortened as GdW_{30} – see Figure 1.7), respectively [36]. Both compounds are characterized by having a single Gd^{3+} ion per molecular unit, providing therefore a relatively large spin ground

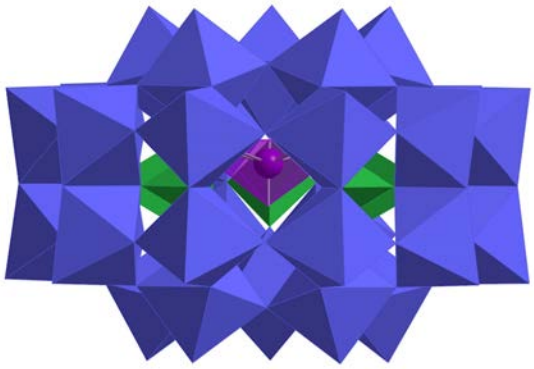

Fig. 1.7. Molecular structure of the GdW_{30} polyoxometalate salt

state and small magnetic anisotropy. Importantly, each magnetic ion is encapsulated by a closed POM framework, which acts as a capping ligand. The resulting intermolecular distances are exceptionally large, reaching 10 Å for GdW_{10} and 20 Å for GdW_{30}. By chemically engineering the molecules in such a way, one can achieve an effective screening of all magnetic interactions and therefore a suitable refrigerant for ultra-low temperatures. This is supported by experiments since magnetic ordering is reported to occur only at 36 mK in the case of GdW_{10}, while the more diluted GdW_{30} is the best realization of a paramagnetic single-atom gadolinium compound because it remains paramagnetic down to the accessed lowest $T \simeq 10$ mK. The inherent downside of such an approach is related to the heavy structural POM framework of each molecular unit that, being non-magnetic and anticipating the discussion presented in the following section, ultimately lowers the efficiency of these refrigerants. The search for other mononuclear molecular isotropic nanomagnets having lighter capping ligands, yet effective in screening all magnetic interactions, should motivate further studies.

1.4.3 Magnetic Density and Choice of Units

As the name tells, the magnetocaloric effect is 'magnetic'. For any refrigerant material, this obvious remark implies nothing but cooling driven by the magnetic elements solely, while the remaining majority of constituting elements participate passively in the physical process. The first step towards the application is the self cooling of the refrigerant material itself: the magnetic elements have to cool the non-magnetic ones, indeed. Therefore, in order to successfully design an ideal refrigerant material one should maximize the magnetic:non-magnetic ratio – for instance, by making use of light ligands interconnecting the magnetic centers.

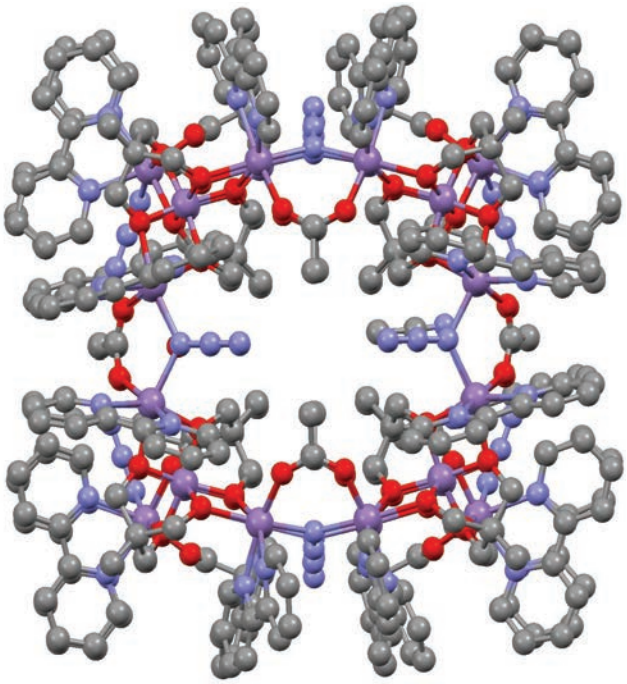

Fig. 1.8. Molecular structure of $\{Mn_8^{4+}Mn_{24}^{2+}\}$. Mn^{4+} and Mn^{2+} = violet, N = light blue, O = red, C = gray. H atoms are omitted for clarity

So far, we have expressed the magnetic entropy change ΔS_m in terms of the *molar* gas constant $R \simeq 8.314$ J mol^{-1} K^{-1} since this has facilitated us in focusing on parameters, such as anisotropy and interactions, that determine the MCE. However, the most common choice of units for ΔS_m is J kg^{-1} K^{-1}. By including the *mass*, these units carry information on the relative amount of magnetic elements. Furthermore from a practical standpoint, an engineer dealing with the development of an adiabatic demagnetization refrigerator would prefer to know the amount of refrigerant material which can be employed per unit of *volume*. The third option, which is then better suited for assessing the applicability of a refrigerant material, consists in expressing the volumetric $\rho\Delta S_m$, where ρ is the mass density of the material, in terms of mJ cm^{-3} K^{-1} units. On this point, one could correctly argue that the MCE of molecule-based refrigerant materials is disfavored by their typically low ρ – though it is not always the case, as exemplified below.

The experimentally-observed maximum value of the entropy change has experienced a terrific escalation in the recent literature. Numerous publications break records and report comparison tables or graphs containing the ΔS_m of several compounds. However, we point out that the impression that the reader could get from such comparisons may be mislead by the choice of

units employed for ΔS_m. To better illustrate how arbitrary and yet how important are the units of measurement, let us consider the following examples.

Case Example: $\{Mn_8^{4+}Mn_{24}^{2+}\}$ *Molecular Nanomagnet*

Let us start by considering the high-nuclearity cluster $\{Mn_8^{4+}Mn_{24}^{2+}\}$, whose magnetically-relevant molecular structure [61] consists of eight planar "centered triangles" composed of a central Mn^{4+} spin center, with $s = 3/2$, antiferromagnetically coupled to three peripheral Mn^{2+} spin centers, each having $s = 5/2$ (Fig. 1.8). Within the molecule, eight triangular clusters are weakly coupled together in the form of a truncated cube by azide and carboxylate ligands. Each $\{Mn_8^{4+}Mn_{24}^{2+}\}$ core is also surrounded by one and a half non-coordinated $[Mn(bpy)_3]^{2+}$. The full formula of the complex reads $\{Mn(bpy)_3\}_{1.5}[Mn_{32}(thme)_{16}(bpy)_{24}(N_3)_{12}(OAc)_{12}](ClO_4)_{11}$ [61]. The magnetocaloric investigations of $\{Mn_8^{4+}Mn_{24}^{2+}\}$ reported a maximum value $-\Delta S_m = 23.2\ R$ at $T \simeq 1.6$ K for $\mu_0\Delta H = (7-0)$ T, which reduces to $-\Delta S_m = 10.0\ R$ at $T = 0.5$ K for $\mu_0\Delta H = (1-0)$ T field change [20]. For widespread applications, the interest is chiefly restricted to applied fields which can be produced with permanent magnets, viz., in the range $1-2$ T. The important remark here is the extremely large values for the entropy change in units of R. Obviously, this is the result of the high spin-nuclearity which favors a correspondingly large magnetic entropy according to Eq. 1.12. Taking into account the molecular mass $m = 11,232.47$ g mol^{-1} of $\{Mn_8^{4+}Mn_{24}^{2+}\}$, the 'new' though equivalent values of the entropy change read $-\Delta S_m = 18.2$ J kg^{-1} K^{-1} and 7.5 J kg^{-1} K^{-1} for $\mu_0\Delta H = (7-0)$ T and $(1-0)$ T, respectively. Finally, to complete our analysis, we consider its mass density $\rho = 1.37$ g cm^{-3} which provides $-\rho\Delta S_m \simeq 25.0$ mJ cm^{-3} K^{-1} and 10.3 mJ cm^{-3} K^{-1} for $\mu_0\Delta H = (7-0)$ T and $(1-0)$ T, respectively.

Case Example: $\{Gd_2\}$ *Molecular Nanomagnet*

Next, we focus on the gadolinium acetate tetrahydrate, $[Gd_2(OAc)_6(H_2O)_4] \cdot 4H_2O$, hereafter shortened as $\{Gd_2\}$ (see Figure 1.9), which is a second example of a molecular cluster, though the nuclearity strongly decreases to just a mere Gd^{3+}-Gd^{3+} ferromagnetic dimer [27]. Because of the low nuclearity, $-\Delta S_m$ does not exceed $\approx 4.0\ R$ at $T \simeq 1.8$ K for $\mu_0\Delta H = (7-0)$ T, which is nearly six times smaller than in $\{Mn_8^{4+}Mn_{24}^{2+}\}$. However, this scenario changes drastically after considering the $\{Gd_2\}$ molecular mass $m = 812.89$ g mol^{-1}, since the latter yields $-\Delta S_m = 40.6$ J kg^{-1} K^{-1} and 27.0 J kg^{-1} K^{-1} for $\mu_0\Delta H = (7-0)$ T and $(1-0)$ T, respectively (Fig. 1.10). For the sake of information, $\rho = 2.04$ g cm^{-3} for $\{Gd_2\}$, which results in $-\rho\Delta S_m \simeq 82.8$ mJ cm^{-3} K^{-1} and 55.1 mJ cm^{-3} K^{-1} for $\mu_0\Delta H = (7-0)$ T and $(1-0)$ T, respectively, i.e., definitely much higher than in $\{Mn_8^{4+}Mn_{24}^{2+}\}$. Really are these last values so exceptionally large?

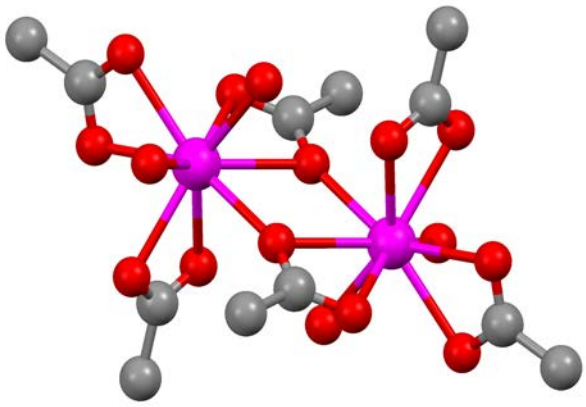

Fig. 1.9. Molecular structure of $\{Gd_2\}$. Gd = purple, O = red, C = gray. H atoms are omitted for clarity

Case Example: GGG *Prototype Material*

Gadolinium gallium garnet (GGG) is *the* reference magnetic refrigerant material for the liquid-helium temperature region [59, 60]. Indeed, its functionality is commercially exploited in spite of a relatively modest maximum $-\Delta S_m = 20.5$ J kg^{-1} K^{-1} for $\mu_0 \Delta H = (2-0)$ T. This apparent contradiction is resolved by measuring the entropy change in terms of equivalent volumetric units, which take into consideration the GGG mass density $\rho = 7.08$ g cm^{-3}. By so-doing, GGG achieves a record value $-\rho\Delta S_m \simeq 145$ mJ cm^{-3} K^{-1} for the same applied field change of 2 T.

Case Example: $\{Gd(OOCH)_3\}_n$ *3D Metal-Organic Framework*

In section 1.3.2, we have introduced the molecule-based $\{Gd(OOCH)_3\}_n$ metal-organic framework material. The MCE of $\{Gd(OOCH)_3\}_n$ was recently determined down to sub-Kelvin temperatures by direct and indirect experimental methods [53]. This three-dimensional MOF is characterized by a relatively compact crystal lattice of weakly interacting Gd^{3+} spin centers interconnected via light formate ligands, overall providing a remarkably large magnetic:non-magnetic elemental weight ratio.

In units of R, the magnetic entropy change is reported to reach the value $-\Delta S_m \approx 2\ R$ at $T \simeq 1.9$ K for $\mu_0 \Delta H = (7-0)$ T. Because of just one Gd^{3+} spin center per formula unit, the maximum experimental value is indeed consistent with the full magnetic entropy, which corresponds to $R \ln(2s+1) = 2.08\ R$, according to Eq. 1.1 for $s = 7/2$. This very modest $-\Delta S_m$ turns out spectacularly large after taking into account the molecular mass $m = 292.30$ g mol^{-1} and mass density $\rho = 3.86$ g cm^{-3} of $\{Gd(OOCH)_3\}_n$. As can be seen in Figure 1.11, the MCE of $\{Gd(OOCH)_3\}_n$ is characterized

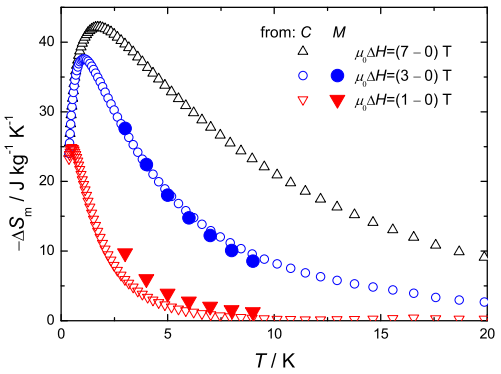

Fig. 1.10. Temperature-dependence of the magnetic entropy change ΔS_m for $\{Gd_2\}$, as obtained from magnetization and specific heat data [27] for the indicated applied-field changes ΔH

by maxima $-\rho\Delta S_m \simeq 120$ mJ cm^{-3} K^{-1} and 189 mJ cm^{-3} K^{-1} for $\mu_0\Delta H = (1-0)$ T and $(3-0)$ T, respectively. These values compare favorably with the ones obtained from GGG and are decidedly superior than in any other molecule-based refrigerant material.

Among the aforementioned examples, which one has the largest MCE?

It should be clear by now that there exist multiple and apparently contradictory answers. If we restrict ourselves to ΔS_m as expressed in R units, then there is no doubt that we should prefer $\{Mn_8^{4+}Mn_{24}^{2+}\}$. However adopting the J kg^{-1} K^{-1} units, $\{Gd_2\}$ and $\{Gd(OOCH)_3\}_n$ perform largely better. Finally, GGG and again $\{Gd(OOCH)_3\}_n$ are far more appealing in the case of volumetric mJ cm^{-3} K^{-1} units. As anticipated, the latter choice of units provides more information since it includes the mass density of the material. In this regard, we note that $\{Gd(OOCH)_3\}_n$ has a very large ρ among molecule-based magnetic materials, though yet smaller than that of GGG. As a matter of fact, the mass density of these two materials is effectively counterbalanced by the magnetic:non-magnetic weight ratio $nA_r/m = 0.54$ and 0.47 for $\{Gd(OOCH)_3\}_n$ and GGG, respectively, where $A_r = 157.25$ g mol^{-1} is the gadolinium relative atomic mass and n is number of Gd^{3+} ions per formula unit, which amounts to 1 in $\{Gd(OOCH)_3\}_n$ and to 3 in GGG. For comparison, the nA_r/m ratio further reduces to 0.39 in the case of $\{Gd_2\}$ for which $n = 2$.

That $\{Gd(OOCH)_3\}_n$ has a larger MCE than the other molecule-based refrigerant materials is also corroborated by the behavior of the adiabatic temperature change, which is strictly related to ΔS_m as we have learnt in section 1.2. For $\mu_0\Delta H = (7-0)$ T, we indeed observe a maximum $\Delta T_{ad} =$

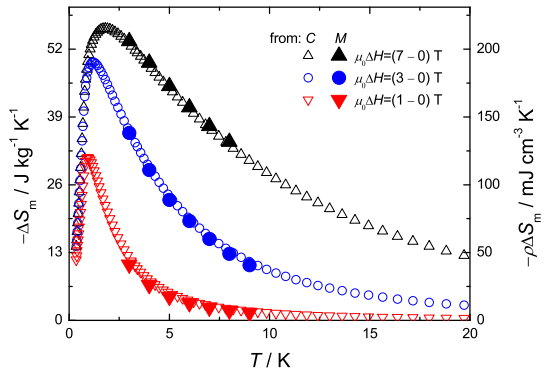

Fig. 1.11. Temperature-dependence of the magnetic entropy change ΔS_m for $\{Gd(OOCH)_3\}_n$, as obtained from magnetization and specific heat data [53] for the indicated applied-field changes ΔH. Vertical axes report units in J kg^{-1} K^{-1} (left) and volumetric mJ cm^{-3} K^{-1} (right)

22.4 K, 12.7 K and 6.7 K for $\{Gd(OOCH)_3\}_n$, $\{Gd_2\}$ and $\{Mn_8^{4+}Mn_{24}^{2+}\}$, respectively [20, 27, 53].

1.5 Towards Applications: On-Chip Refrigeration

Sub-Kelvin microrefrigeration is an emerging trend in cryogenic physics and technology since it allows for the reduction of large quantities of refrigerants [62, 63]. It also has the potential to open up new markets by making available cheap (^{3}He-free) cooling. On-chip devices are expected to find applications as cooling platforms for all those instruments where local refrigeration down to very-low temperatures is needed. These can include, although is not limited to, high-resolution X-ray and gamma-ray detectors for, e.g., astronomy, materials science, and security instrumentation.

In parallel, research on surface-deposited molecular aggregates has been evolving with the aim of assembling and integrating molecules into on-chip functional devices [64]. In this regard, the exploitation of the cooling properties of molecule-based materials is seen as a promising future technology. By developing a suitable silicon-based host device which is adiabatically isolated and has a negligible specific heat in the working temperature range, one could expect to cool from liquid-helium temperature down to milliKelvin, after having provided a field change of a few tesla. This could represent by far the best performance for on-chip cooling. Microrefrigerators based on solid-state electronic schemes, currently studied and developed for low-temperature applications, provide a cooling of the order of $\Delta T \approx 0.1$ K at the very best [63]

– a value notably smaller than that promised by the magnetic molecules. Obviously, for this approach to become a reality, a relatively strong binding of the molecules to the surface and the preservation of their functionalities once deposited are sine-qua-non conditions.

The magnetic investigations on molecule-based coolers have so far been carried out for bulk materials. The target of extending these studies to include molecules deposited onto surfaces is challenging, both for the low temperatures required and, specially, for the relatively small amount of deposited material which results in a weak strength of the magnetic signal.

Case Example: Surface-Deposited $\{Gd_2\}$ *Molecular Nanomagnet*

From the very recent literature [28], we report the first study by magnetic force microscopy (MFM) of molecular coolers deposited on a Si substrate, as an intermediate step towards the interfacing of these molecules with a future Si-based thermal sensor designed to function as a microrefrigerator. This work specifically refers to the $\{Gd_2\}$ molecular nanomagnet (Fig. 1.9) that we already met in section 1.4.3.

The substrate consists of a Si wafer that is p-doped with boron to improve its conductivity and to permit its grounding, particularly important for preventing the accumulation of electric charges during MFM measurements. Previous to surface magnetic measurements, a rational organization of the $\{Gd_2\}$ molecules on the Si substrate is necessary to ensure a proper contrast between magnetic and non-magnetic areas as needed to estimate the magnetic stray field generated by the deposits. For this purpose, dip-pen nanolithography (DPN) is a suitable tip-assisted technique since it has already been shown to precisely place drops of a controlled size according to predefined patterns with sub-micrometer precision [65]. As a last step before the deposition, a clean writing surface is provided by ultrasound in acetonitrile, ethanol and deionized water. This last step also ensures the presence of a thin layer of native oxide, which in turn enables the adsorption of molecular species through hydrogen bonding with hydroxyl groups naturally present at the surface of oxides, even without specific pre-treatment. With its four terminal coordinated water molecules and acetate groups in various coordination modes, the neutral $\{Gd_2\}$ molecule may form a range of hydrogen bonds, either as donor or acceptor, with surface hydroxyls or adsorbed water, as it indeed does in its crystalline form with lattice water molecules [27]. A further advantage of this material resides in a relatively robust, yet light, structural framework surrounding each Gd^{3+} ion. $\{Gd_2\}$ is thus a good candidate to preserve its structure after an efficient grafting to hydrophilic surfaces without pre-functionalization.

Figure 1.12 shows the scheme of the measurements reported in Ref. [28], consisting of a MFM tip positioned at a constant height $\approx$ 150 nm from the Si substrate and a $\{Gd_2\}$ droplet, whose height is $\approx$ 10 nm, while the lengths of the two oval axes are $\approx$ 1.7 μm and $\approx$ 1.4 μm, respectively. The

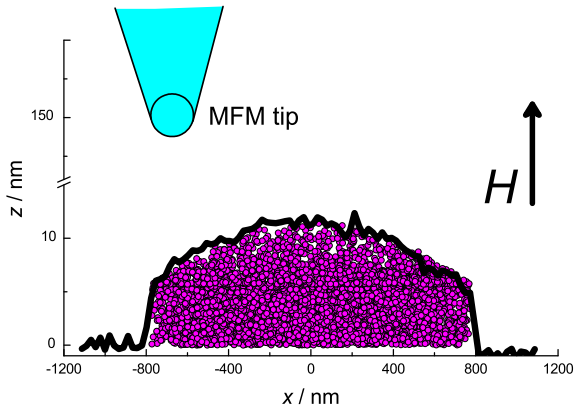

Fig. 1.12. Scheme representing a sampling of $\{Gd_2\}$ molecules (dots) positioned within a droplet delimited by an experimental profile and deposited on the Si substrate (xy plane). The sensing magnetic tip is at constant height $h \approx 150$ nm. The applied field H is oriented along z

applied field is oriented perpendicular to the plane. Figure 1.13 shows the MFM images collected in the frequency shift mode (Δf) at $T = 5.0$ K. The frequency shift measures the gradient of the force acting on the MFM tip and it is here directly proportional to the stray field generated by the drop [28]. Each MFM image is accompanied by the corresponding profile along a line bisecting the droplet. For $H = 0$, no magnetic stray field is expected from the $\{Gd_2\}$ droplet. Therefore, in order to minimize van der Waals contributions, the tip-to-sample distance is set as such to barely see any topography for zero-applied field (see the first panel in Fig. 1.13). The area external to the drop is the non-magnetic contribution of the substrate which constitutes the reference background (dashed lines in the profiles). The tip magnetization is constantly at saturation for all in-field MFM images, since the applied magnetic field largely exceeds the coercive field of the tip ($\approx 5 \times 10^{-2}$ T).

The evolution of magnetic contrast between the $\{Gd_2\}$ droplet and the non-magnetic substrate is well visible in Figure 1.13, as a function of the applied magnetic field. Specifically, the inner area of the drop becomes darker, while the border brighter and thicker, by increasing the field. In order to explain the observed behavior, let us first consider the magnetic field generated by the $\{Gd_2\}$ droplet as represented by lines of induction or flux lines. One can easily understand that the stray-field flux lines gradually change their direction, till reaching the inversion, on approaching the border of the drop. Accordingly, the magnetic interaction between tip and sample changes from attractive to repulsive depending on the orientation of these flux lines, therefore shifting the resonance from lower (darker) to higher (brighter) frequencies,

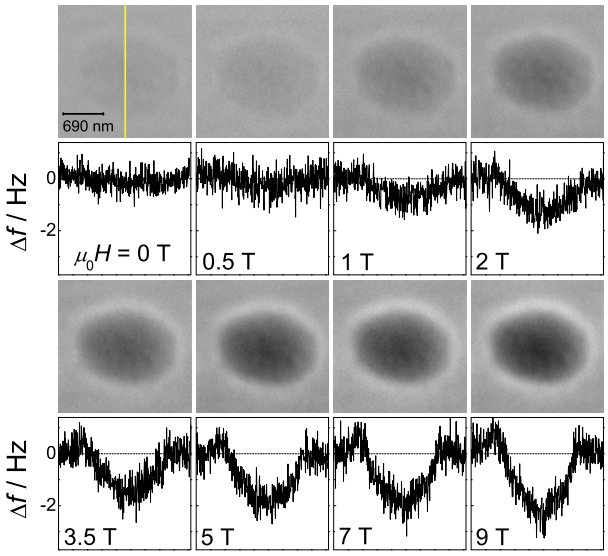

Fig. 1.13. Magnetic images (frequency shift, Δf) of an individual $\{Gd_2\}$ droplet taken at $T = 5.0$ K and different magnetic fields, as labeled. The images are represented in the same contrast scale, namely from -3.4 Hz to 1.5 Hz. Magnetic profiles are presented below each corresponding image, with the background zero-field level being represented by a dotted line

respectively. The profile lines provide further evidence for the dependence of the magnetic contrast on the applied field.

Importantly, a quantitative analysis of the magnetic contrast reveals that the (T, H)-dependence of the Δf measurements can be directly associated to the magnetization of bulk $\{Gd_2\}$, enabling us to conclude that the as-deposited molecules hold intact their magnetic characteristics and, consequently, the cooling functionality as well [28]. Transferring a known, excellent cryogenic magnetocaloric material, such as the $\{Gd_2\}$ molecular nanomagnet, from bulk crystal to a silicon substrate without deterioration of its properties paves the way towards the realization of a molecule-based microrefrigerating device for very low temperatures.

1.6 Concluding Remarks

Over the past couple of years there has been an upsurge in the number of molecule-based materials proposed as enhanced magnetic coolers for cryogenic temperatures. The research has been recently opened to extended three-dimensional structural frameworks, which will allow taking advantage of both the chemical variety and intrinsic robustness of MOF materials. However,

in spite of the many efforts devoted so far to this end, there are still challenges to overcome before molecule-based magnetic coolers find widespread applications. For instance, sizeable intermolecular magnetic correlations and intrinsically low thermal conductivities are two issues that limit their applicability, especially at very low temperatures. New solutions are proposed and explored by combining chemical synthesis with materials science and advanced instrumentation techniques. There is a promising research future on grafting molecule-based magnetic coolers to substrates with a high thermal conductivity. One can envision that in a not-too-distant future, devices of reduced sizes will exploit the cooling functionality of these molecules.

Acknowledgements

This work would not have been possible without the contribution of, in alphabetical order: E. K. Brechin, A. Camón, D. Collison, E. Coronado, E. J. L. McInnes, G. Lorusso, F. Luis, L. J. de Jongh, E. Palacios, O. Roubeau, D. Ruiz-Molina and R. Sessoli. Financial support by the Spanish MINECO through grant MAT2012-38318-C03-01 is acknowledged.

References

1. E. Warburg, Ann. Phys. **13**, 141 (1881)
2. P. Weiss and A. Piccard, Compt. Rend. Ac. Sc. **166**, 352 (1918)
3. P. Debye, Ann. Phys. **81**, 1154 (1926)
4. W. F. Giauque, J. Am. Chem. Soc. **49**, 1864 (1927)
5. W. F. Giauque and D. P. MacDougall, Phys. Rev. **43**, 768 (1933)
6. See, e.g., R. P. Hudson, *Principles and Application of Magnetic Cooling*, (North-Holland Publishing Company, Amsterdam, 1972)
7. See, e.g., F. Pobell, *Matter and Methods at Low Temperatures*, 3rd edn. (Springer-Verlag, Berlin Heidelberg, 2007)
8. Yu. I. Spichkin, A. K. Zvezdin, S. P. Gubin, A. S. Mischenko and A. M. Tishin, J. Phys. D: Appl. Phys. **34**, 1162 (2001)
9. F. Torres, J. M. Hernández, X. Bohigas and J. Tejada, Appl. Phys. Lett. **77**, 3248 (2000)
10. M. Affronte, A. Ghirri, S. Carretta, G. Amoretti, S. Piligkos, G. A. Timco and R. E. P. Winpenny, Appl. Phys. Lett. **84**, 3468 (2004)
11. M. Evangelisti, A. Candini, A. Ghirri, M. Affronte, E. K. Brechin and E. J. L. McInnes, Appl. Phys. Lett. **87**, 072504 (2005)
12. M. Evangelisti, A. Candini, A. Ghirri, M. Affronte, S. Piligkos, E. K. Brechin and E. J. L. McInnes, Polyhedron **24**, 2573 (2005)
13. R. Shaw, R. H. Laye, L. F. Jones, D. M. Low, C. Talbot-Eeckelaers, Q. Wei, C. J. Milios, S. Teat, M. Helliwell, J. Raftery, M. Evangelisti, M. Affronte, D. Collison, E. K. Brechin and E. J. McInnes, Inorg. Chem. **46**, 4968 (2007)
14. E. Manuel, M. Evangelisti, M. Affronte, M. Okubo, C. Train and M. Verdaguer, Phys. Rev. B **73**, 172406 (2006)

15. M. Evangelisti, E. Manuel, M. Affronte, M. Okubo, C. Train and M. Verdaguer, J. Magn. Magn. Mater. **316**, e569 (2007)
16. M. Manoli, R. D. L. Johnstone, S. Parsons, M. Murrie, M. Affronte, M. Evangelisti and E. K. Brechin, Angew. Chem. Int.-Ed. **46**, 4456 (2007)
17. M. Manoli, A. Collins, S. Parsons, A. Candini, M. Evangelisti and E. K. Brechin, J. Am. Chem. Soc. **130** 11129 (2008)
18. G. Karotsis, M. Evangelisti, S. J. Dalgarno and E. K. Brechin, Angew. Chem. Int.-Ed. **48**, 9928 (2009)
19. G. Karotsis, S. Kennedy, S. J. Teat, C. M. Beavers, D. A. Fowler, J. J. Morales, M. Evangelisti, S. J. Dalgarno and E. K. Brechin, J. Am. Chem. Soc. **132**, 12983 (2010)
20. M. Evangelisti, A. Candini, M. Affronte, E. Pasca, L. J. de Jongh, R. T. W. Scott and E. K. Brechin, Phys. Rev. B **79**, 104414 (2009)
21. L. Sedláková, J. Hanko, A. Orendčov, M. Orendáč, C. L. Zhou, W. H. Zhu, B. W. Wang, Z. M. Wang and S. Gao, J. Alloys Compd. **487**, 425 (2009)
22. S. Nayak, M. Evangelisti, A. K. Powell and J. Reedijk, Chem. Eur. J. **16**, 12865 (2010)
23. J. W. Sharples, Y. Z. Zheng, F. Tuna, E. J. McInnes and D. Collison, Chem. Commun. **47**, 7650 (2011)
24. J.-L. Liu, J.-D. Leng, Z. Lin and M.-L. Tong, Chem. Asian J. **6**, 1007 (2011)
25. Y. Z. Zheng, M. Evangelisti and R. E. P. Winpenny, Angew. Chem. Int.-Ed. **50**, 3692 (2011)
26. J. B. Peng, Q. C. Zhang, X. J. Kong, Y. P. Ren, L. S. Long, R. B. Huang, L. S. Zheng and Z. P. Zheng, Angew. Chem. Int.-Ed. **50**, 10649 (2011)
27. M. Evangelisti, O. Roubeau, E. Palacios, A. Camón, T. N. Hooper, E. K. Brechin and J. J. Alonso, Angew. Chem. Int.-Ed. **50**, 6606 (2011)
28. G. Lorusso, M. Jenkins, P. González-Monje, A. Arauzo, J. Sesé, D. Ruiz-Molina, O. Roubeau and M. Evangelisti, Adv. Mater. **25**, 2984 (2013)
29. S. K. Langley, N. F. Chilton, B. Moubaraki, T. Hooper, E. K. Brechin, M. Evangelisti and K. S. Murray, Chem. Sci. **2**, 1166 (2011)
30. A. Hosoi, Y. Yukawa, S. Igarashi, S. J. Teat, O. Roubeau, M. Evangelisti, E. Cremades, E. Ruiz, L. A. Barrios and G. Aromí, Chem. Eur. J. **17**, 8264 (2011)
31. Y. Z. Zheng, M. Evangelisti and R. E. P. Winpenny, Chem. Sci. **2**, 99 (2011)
32. F. S. Guo, J. D. Leng, J. L. Liu, Z. S. Meng and M. L. Tong, Inorg. Chem. **51**, 405 (2012)
33. Y. Z. Zheng, M. Evangelisti, F. Tuna and R. E. P. Winpenny, J. Am. Chem. Soc. **134**, 1057 (2012)
34. E. Cremades, S. Gomez-Coca, D. Aravena, S. Alvarez and E. Ruiz, J. Am. Chem. Soc. **134**, 10532 (2012)
35. J. D. Leng, J. L. Liu and M. L. Tong, Chem. Commun. **48**, 5286 (2012)
36. M.-J. Martínez-Pérez, O. Montero, M. Evangelisti, F. Luis, J. Sesé, S. Cardona-Serra and E. Coronado, Adv. Mater. **24**, 4301 (2012)
37. T. N. Hooper, J. Schnack, S. Piligkos, M. Evangelisti and E. K. Brechin, Angew. Chem. Int.-Ed. **51**, 4633 (2012)
38. P.-F. Shi, Y.-Z. Zheng, X.-Q. Zhao, G. Xiong, B. Zhao, F.-F. Wan and P. Cheng, Chem. Eur. J. **18**, 15086 (2012)
39. T. Birk, K. S. Pedersen, C. Aa. Thuesen, T. Weyhermüller, M. Schau-Magnussen, S. Piligkos, H. Weihe, S. Mossin, M. Evangelisti and J. Bendix, Inorg. Chem. **51**, 5435 (2012)

40. C. Aa. Thuesen, K. S. Pedersen, M. Schau-Magnussen, M. Evangelisti, J. Vibenholt, S. Piligkos, H. Weihea and J. Bendix, Dalton Trans. **41**, 11284 (2012)
41. J.-B. Peng, Q.-C. Zhang, X.-J. Kong, Y.-Z. Zheng, Y.-P. Ren, L.-S. Long, R.-B. Huang, L.-S. Zheng and Z. Zheng, J. Am. Chem. Soc. **134**, 3314 (2012)
42. G. Lorusso, M. A. Palacios, G. S. Nichol, E. K. Brechin, O. Roubeau and M. Evangelisti, Chem. Commun. **48**, 7592 (2012)
43. F.-S. Guo, Y.-C. Chen, J.-L. Liu, J.-D. Leng, Z.-S. Meng, P. Vrábel, M. Orendáč and M.-L. Tong, Chem. Commun. **48**, 12219 (2012)
44. A. S. Dinca, A. Ghirri, A. M. Madalan, M. Affronte and M. Andruh, Inorg. Chem. **51**, 3935 (2012)
45. R. Sibille, T. Mazet, B. Malaman, T. Gaudisson and M. François, Inorg. Chem. **51**, 2885 (2012)
46. M. Fitta, M. Balanda, M. Mihalik, R. Pelka, D. Pinkowicz, B. Sieklucka and M. Zentkova, J. Phys.: Condens. Matter **24**, 506002 (2012)
47. R. Sibille, T. Mazet, B. Malaman and M. François, Chem. Eur. J. **18**, 12970 (2012)
48. Y. Zheng, Q.-C. Zhang, L.-S. Long, R.-B. Huang, A. Müller, J. Schnack, L.-S. Zhenga and Z. Zhenga, Chem. Commun. **49**, 36 (2013)
49. I. A. Gass, E. K. Brechin and M. Evangelisti, Polyhedron **52**, 1177 (2013)
50. L.-X. Chang, G. Xiong, L. Wang, P. Cheng and B. Zhao, Chem. Commun. **49**, 1055 (2013)
51. Z.-Y. Li, J. Zhu, X.-Q. Wang, J. Ni, J.-J. Zhang, S.-Q. Liu and C.-Y. Duan, Dalton Trans. **42**, 5711 (2013)
52. E. M. Pineda, F. Tuna, R. G. Pritchard, A. C. Regan, R. E. P. Winpenny and E. J. L. McInnes, Chem. Commun. **49**, 3522 (2013)
53. G. Lorusso, J. W. Sharples, E. Palacios, O. Roubeau, E. K. Brechin, R. Sessoli, A. Rossin, F. Tuna, E. J. L. McInnes, D. Collison and M. Evangelisti, Adv. Mater. (2013), DOI: 10.1002/adma.201301997
54. E. Colacio, J. Ruiz, G. Lorusso, E. K. Brechin and M. Evangelisti, Chem. Commun (2013), **49**, 3845 (2013)
55. See, e.g., C. Kittel, *Introduction to Solid-State Physics*, 8th edn. (John Wiley & Sons, Inc., New York, 2005)
56. V. K. Pecharsky and K. A. Geschneidner Jr., J. Appl. Phys. **86**, 565 (1999)
57. V. K. Pecharsky and K. A. Gschneidner Jr., J. Mag. Mag. Mater. **200**, 44 (1999)
58. R. F. Wielinga, J. Lubbers and W. J. Huiskamp, Physica **37**, 375 (1967)
59. B. Daudin, R. Lagnier and B. Salce, J. Magn. Magn. Mater. **27**, 315 (1982)
60. T. Numazawa, K. Kamiya, T. Okano and K. Matsumoto, Physica B **329-333**, 1656 (2003)
61. R. T. W. Scott, S. Parsons, M. Murugesu, W. Wernsdorfer, G. Christou and E. K. Brechin, Angew. Chem. Int. Ed. **44**, 6540 (2005)
62. F. Giazotto, T. T. Heikkilä, A. Luukanen, A. M. Savin and J. P. Pekola, Rev. Mod. Phys. **78**, 217 (2006)
63. J. T. Muhonen, M. Meschke and J. P. Pekola, Rep. Prog. Phys. **75**, 046501 (2012)
64. N. Domingo, E. Bellido and D. Ruiz-Molina, Chem. Soc. Rev. **41**, 258 (2012)
65. A. Martínez-Otero, P. González-Monje, D. Maspoch, J. Hernando and D. Ruiz-Molina, Chem. Commun. **47**, 6864 (2011)